EurJIC
European Journal of Inorganic Chemistry

Chemistry Europe
European Chemical Societies Publishing

Accepted Article

Title: A Strongly Coupled Biruthenium Complex as Catalyst for the Water Oxidation Reaction

Authors: Sofia E. Dominguez, Virginia M. Juarez, German E. Pieslinger, and Luis M. Baraldo

To be cited as: *Eur. J. Inorg. Chem.* 10.1002/ejic.202100843

Link to VoR: https://doi.org/10.1002/ejic.202100843

WILEY-VCH

10.1002/ejic.202100843

A Strongly Coupled Biruthenium Complex as Catalyst for the Water Oxidation Reaction

Sofía E. Domínguez,[a],[b] M. Virginia Juarez,[a],[b] German E. Pieslinger,[a],[c] and Luis M. Baraldo*[a],[b]

[a] Dr. S. E. Dominguez, M. V. Juarez, Dr. G. E. Pieslinger, Prof. Dr. L. M. Baraldo
Universidad de Buenos Aires. Facultad de Ciencias Exactas y Naturales. Departamento de Química Inorgánica, Analítica y Química Física. Buenos Aires, Argentina.
E-mail: baraldo@qi.fcen.uba.ar

[b] Dr. S. E. Dominguez, M. V. Juarez, Prof. Dr. L. M. Baraldo
CONICET - Universidad de Buenos Aires. Instituto de Química Física de Materiales, Ambientes y Energía (INQUIMAE). Buenos Aires, Argentina.

[c] Dr. G. E. Pieslinger
CONICET − Universidad de Buenos Aires. Instituto de Química y Fisicoquímica Biológicas (IQUIFIB). Buenos Aires, Argentina.

Dedicated to Prof. José A. Olabe on occasion of his 80th birthday

Abstract: The catalytic activity towards water oxidation of a strongly coupled bimetallic ruthenium complex, *trans*-[Ru(tpy)(bpy)(μ-CN)Ru(py)$_4$(OH$_2$)]$^{3+}$ (**Ru^{II}Ru^{II}OH$_2$**), where tpy = 2,2′:6′,2′′-terpyridine, bpy = 2,2′-bipyridine and py = pyridine are presented. At pH 1 the first two oxidation reactions are centred at the aquo fragment and result in the **Ru^{II}Ru^{III}OH$_2$** and **Ru^{II}Ru^{IV}O** redox states as confirmed by its spectroscopy and DFT calculations. Oxidation by an additional electron is followed by an irreversible step and a catalytic wave associated with the water oxidation reaction. At pH 1 the reaction with an excess of Ce(IV) results in the generation of an stoichiometric amount of oxygen based on molar amounts of the added Ce(IV). The dominant species during the catalytic cycle is the three-electron oxidized product, **Ru^{III}Ru^{IV}O**. The reduction of the concentration of Ce(IV) monitored at 370 nm follow the rate equation, $-d[Ce(IV)]/dt = k_{ox}[Ce(IV)][\mathbf{Ru^{II}Ru^{II}OH_2}]$ with a $k_{ox} = 82 \pm 3$ M^{-1}s^{-1} at T = 298 K. The **Ru^{III}Ru^{IV}O** species is not stable and reacts to give **Ru^{II}Ru^{IV}O**.

Introduction

The storage of energy from renewable sources as high-energy-density fuels could alleviate the challenges that accompany large-scale use of intermittent energy sources, such as solar and eolic.[1] One such process is the splitting of water in H_2 and O_2 as shown in eq 1.

$$2\ H_2O \rightarrow 2\ H_2 + O_2 \qquad E° = 1.23\ V\ vs\ NHE\ (1)$$

One of the reactions involved in this process is water oxidation. This reaction is challenging as involves an oxidation by four electrons, the removal of four protons and the formation of a O-O bond.[2] These requirements often result in high overpotentials that diminishes the efficiency of the reaction and hence are important for practical applications.[3]

For these reasons much effort has been devoted to explore new molecular catalysts in order to facilitate this reaction and tremendous progress have been achieved in the last years.[4,5] Simple ruthenium polypyridyl complexes are among the more stable and active water oxidation molecular catalyst under a variety of conditions. The accepted mechanism for this reaction involves the generation of a electrophilic Ru^{V}O moiety,[6] although it has been reported that Ru^{IV}O can also be active catalyst when its coordination sphere is occupied by relative poor electron-donating ligands.[7]

Coupling of a redox centre to a Ru catalyst could provide another way to store an oxidation equivalent avoiding the need to reach a Ru^{V}O oxidation state. This would be especially effective if both centres are strongly coupled. Cyanide bridge is among the most explored bridges in the literature, and it can promote a strong coupling demonstrated by its ability to promote charge delocalization in diruthenium mixed-valence complexes.[8–11]

In this work, we show that the strongly coupled biruthenium complex *trans*-[Ru(tpy)(bpy)(μ-CN)Ru(py)$_4$(OH$_2$)]$^{3+}$ (**Ru^{II}Ru^{II}OH$_2$**, where tpy = 2,2':6',2''-terpyridine, bpy = 2,2′-bipyridine and py = pyridine) can also act as an active water oxidation catalyst for the reaction with an excess of Ce(IV) at pH 1. The rate determining step of the reaction is first order both in Ce(IV) and **Ru^{II}Ru^{II}OH$_2$** and we assign the resting state of the catalytic cycle as the three-electron oxidized complex *trans*-[Ru^{III}(tpy)(bpy)(μ-CN)Ru^{IV}(py)$_4$=O]$^{3+}$ (**Ru^{III}Ru^{IV}=O**). Hence, the rate-determining step is the oxidation of **Ru^{III}Ru^{IV}=O** by Ce(IV) and this process is probably coupled with the water nucleophilic attack on the Ru-oxo group.

Results and Discussion

The complex $[Ru(tpy)(bpy)(\mu\text{-}CN)Ru(py)_4(OH_2)]^{3+}$ (**$Ru^{II}Ru^{II}OH_2$**, Scheme 1) was prepared by a slight modification of the reported procedure[8] involving the reaction of nitrosyl complex with azide under argon in aqueous solution (see Supporting Information for details).

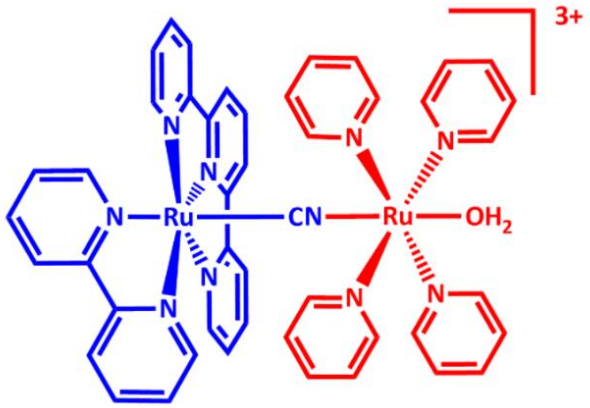

Scheme 1. Structure of the biruthenium aquo complex $[Ru(tpy)(bpy)(\mu\text{-}CN)Ru(py)_4(OH_2)]^{3+}$ (**$Ru^{II}Ru^{II}OH_2$**) studied in this work.

Electrochemistry

Figure 1 shows cyclic voltammetry experiments of a solution of **$Ru^{II}Ru^{II}OH_2$** in 0.1 M trifluoroacetic acid with 7 % propylene carbonate and Table 1 collect the redox potential for all the relevant species. The oxidative scan shows two processes followed by a third that is mounted on a catalytic wave. The second oxidation wave is reversible at low scan rates (Figure S3, S15 and S16) and begins to be less defined at hight scan rates. This behaviour is typical of the slow kinetics at the electrode of a Ru^{IV}/Ru^{III} couple.[12,13] The third oxidation wave is reversible at high scan rates (Figure 1, left), but becomes irreversible at slower scan rates (Figure S3). This indicates the presence of a chemical process that consumes the three-electron oxidized product. At pH 7 the first two processes are shifted to lower potentials, while the third oxidation appears as a completely irreversible process at the same potential on top of a pronounced catalytic wave (Figure 1, right).

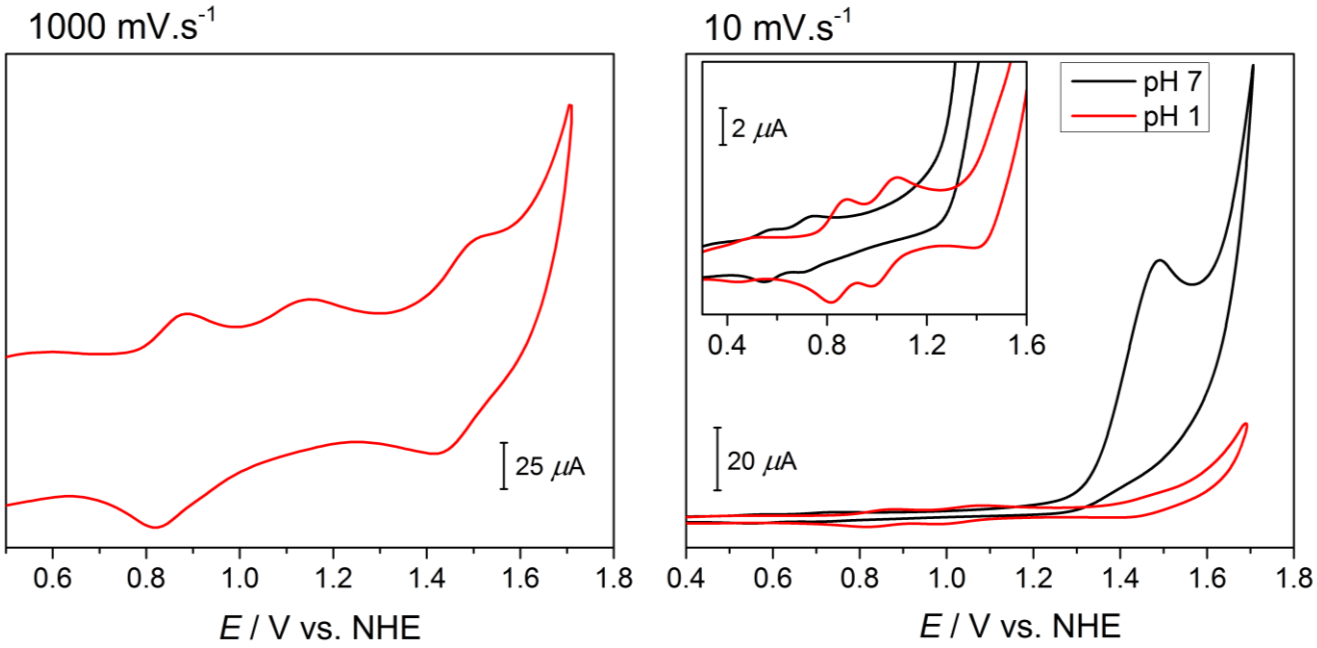

Figure 1. Left: cyclic voltammograms of **$RuRuOH_2$** at pH 1 (scan rate = 1000 mV/s). Right: cyclic voltammograms with scan rate = 10 mV/s at pH 1 and 7.

Table 1. Summary of the Electrochemical Properties for **RuRuOH₂** at 10 mV·s^{-1} scan rate. † = 500 mV·s^{-1} scan rate. § = E_a. (E vs. NHE)

	$E_{1/2}(E_a - E_c)$/V (mV)		
	$Ru_{py}^{III/II}$	$Ru_{py}^{IV/III}$	$Ru_{pp}^{III/II}$
pH 1	0.85 (59)	1.03 (95)	1.47 (75)†
pH 7	0.57 (57)	0.72 (53)	1.49 §

A more detailed exploration of the dependence of the electrochemistry with the pH (Figure 2) allows us to assign the observed redox processes. Between pH 1 and pH 2 the difference on the redox potential for both processes increases, while above pH 2 they decrease parallel to each other with a slope close to 0.059 V/pH as expected for a change in the proton content of the species involved for both processes. These observations are compatible the following reactions:

Below pH 1:

$$[Ru^{II}Ru^{III}OH_2]^{4+} + 1\ e^- \rightleftharpoons [Ru^{II}Ru^{II}OH_2]^{3+}$$

$$[Ru^{II}Ru^{IV}O]^{3+} + 2\ H^+ + 1\ e^- \rightleftharpoons [Ru^{II}Ru^{III}OH_2]^{4+}$$

Above pH 2:

$$[Ru^{II}Ru^{III}OH]^{3+} + H^+ + 1\ e^- \rightleftharpoons [Ru^{II}Ru^{II}OH_2]^{3+}$$

$$[Ru^{II}Ru^{IV}O]^{3+} + H^+ + 1\ e^- \rightleftharpoons [Ru^{II}Ru^{III}OH]^{3+}$$

The third oxidation wave is mainly pH independent although its position is difficult to define as it becomes increasingly irreversible and less defined at higher pH. We assign this process as the one-electron oxidation centred at the chromophore.

$$[Ru^{III}Ru^{IV}O]^{4+} + 1\ e^- \rightleftharpoons [Ru^{II}Ru^{IV}O]^{3+}$$

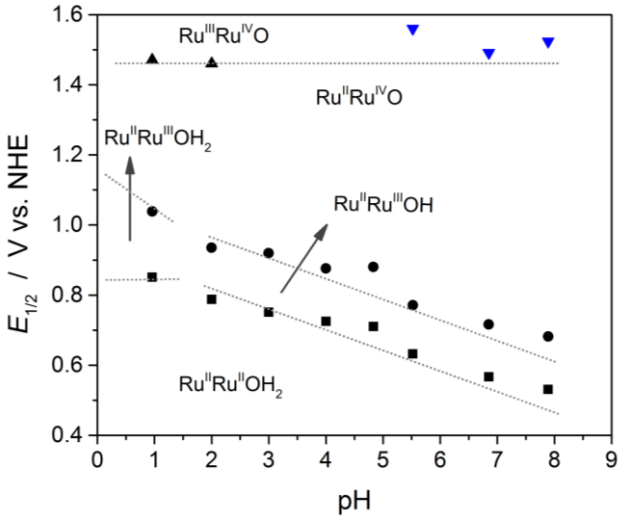

Figure 2. Plots of $E_{1/2}$ (V vs NHE) vs pH for the three redox couples of (**1**) in aqueous solution (I = 0.1 M; T = 298 K; glassy carbon working electrode). The (▼) correspond to the anodic peak as the process becomes irreversible at this pH.

Vis-NIR spectroscopy

To gain more information on the nature of the species involved in the redox reactions at different pHs we performed spectroelectrochemistry experiments at pH 1 and 7 (Figure 3). The visible spectrum of **$Ru^{II}Ru^{II}OH_2$** is identical at both pHs and is dominated by two sets of metal-to-ligand charge transfer (MLCT) transitions (Table 2) from both Ru centres to the aromatic ligands as observed for other complexes of the $[Ru(tpy)(bpy)(\mu\text{-}CN)Ru(py)_4L]^{3+}$ family.[8] The more intense transition at 28100 cm^{-1} corresponds

to the {Ru(py)$_4$} fragment, while the weaker band shifted to the red at 23000–22000 cm^{-1} is associated with the {Ru(tpy)(bpy)} chromophore.

Upon one electron oxidation at pH 1 the band at 28100 cm^{-1} disappears and a new band is developed in the NIR at 9500 cm^{-1}. The latter is an intervalence charge transfer (IVCT) band as expected for a mixed-valence complex, while the disappearance of the band at 28100 cm^{-1} confirms that the oxidation is centred in the {Ru(py)$_4$} moiety. As observed previously,[8] the MLCT band centred at the {Ru(tpy)(bpy)} fragment shifts to higher energies (Table 1) due to the influence of the Ru(III) moiety attached to the cyanide bridge. At pH 7 the oxidation by one electron also results in the disappearance of the band at 28100 cm^{-1}, but in this case the IVCT band appears at 14600 cm^{-1}. This shift is associated with the deprotonation of the aquo ligand in the {Ru(py)$_4$} fragment at this pH as assigned by the pH dependence of the redox potentials involving this species. The energy shift to higher energy is compatible with the stabilization of Ru(III) by OH$^-$ ligand.

Oxidation by a second electron gives a spectrum that is identical at both pHs. In this spectrum the IVCT at low energy is lost, but the MLCT band is still clearly visible at 22800 cm^{-1}. This leads us to assign the configuration of this species as **Ru^{II}Ru^{IV}O**.

Table 2. Experimental vis-NIR data in aqueous solution 0.1 M for the redox species associated with **RuRuOH$_2$**. Only bands that are resolved in experimental spectra are included.

		ν_{max} / 10^3 cm^{-1} (ε_{max} /10^3 M^{-1} cm^{-1})		
Complex	Redox State	MLCT dπ(Ru) → π*(py)	MLCT dπ(Ru) → π*(pp)	IVCT
RuRuOH$_2$	[II,II]	28.1 (20.2)	22.8 (8.8) sh	
RuRuOH$_2$	[II,III]		23.9 (6.7)	9.5 (3.5)
RuRuOH	[II,III]		22.8 (8.8)	14.6 (2.6)
RuRuO	[II,IV]		22.9 (10.0)	20.4 (5.7) sh

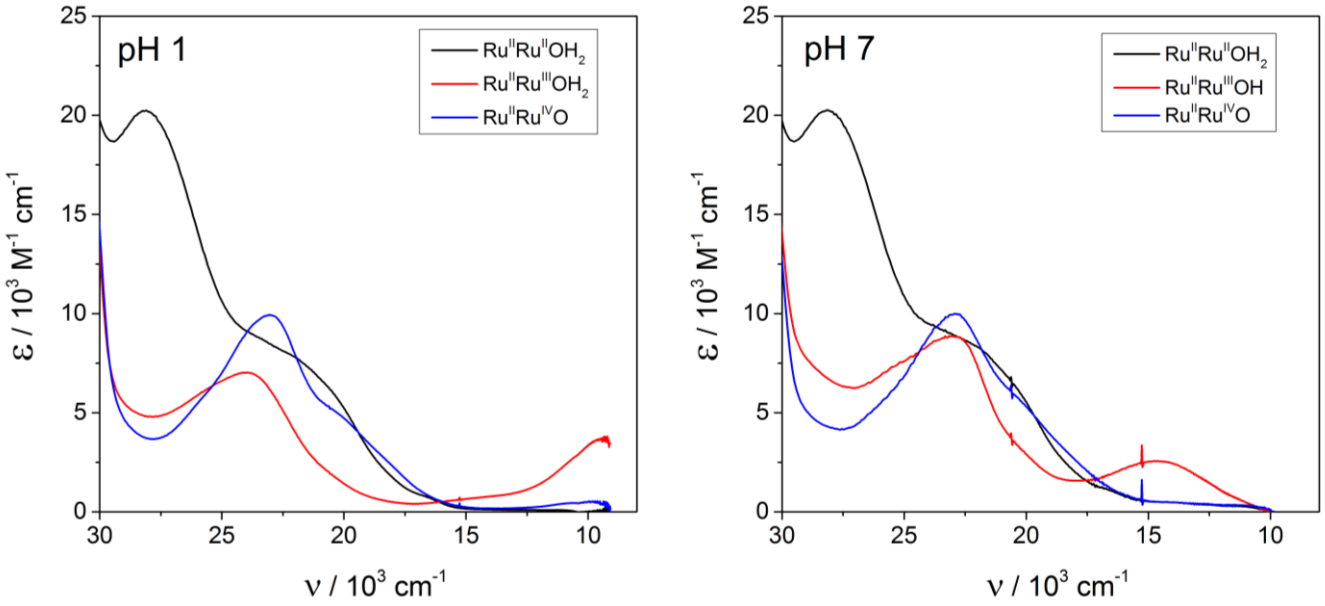

Figure 3. Vis−NIR spectra for the **Ru^{II}Ru^{II}OH$_2$** (black), **Ru^{II}Ru^{III}OH$_2$** (red), and **Ru^{II}Ru^{IV}O** (blue) obtained through spectroelectrochemical experiments at pH 1.0, 0.1 M HClO$_4$ (left), and for **Ru^{II}Ru^{II}OH$_2$** (black), **Ru^{II}Ru^{III}OH** (red), and **Ru^{II}Ru^{IV}O** (blue) at pH 7 (right)

(TD)DFT calculations.

(TD)DFT calculations have shown to be a very useful tool to understand the spectroscopy of Ru-Ru cyanide bridged complexes in different oxidation states.[8–10,14,15] Figure 4 shows that the calculated spectra reproduce well the main features of the experimental

spectra for **$Ru^{II}Ru^{II}OH_2$**, **$Ru^{II}Ru^{III}OH$**, **$Ru^{II}Ru^{III}OH_2$** and **$Ru^{II}Ru^{IV}O$** including the shift to higher energy of the IVCT observed upon deprotonation of **$Ru^{II}Ru^{III}OH_2$**.

(TD)DFT calculation indicates that the unpaired electron in complex **$Ru^{II}Ru^{III}OH_2$** is substantially delocalized between both Ru ions through the interaction promoted by the cyanide bridge (Figure S4). As observed for related mixed-valence cyanide-bridged diruthenium polypyridines the calculated energy for the IVCT transition is lower than the observed one, which is indicative of a DFT overestimation of the delocalization compared to the experimental one.[15] This overestimation is also expressed in the higher energy calculated for the MLCT transition, as the calculations assigns a larger Ru(III) character to {Ru(tpy)(bpy)} fragment than what is observed experimentally. For the **$Ru^{II}Ru^{III}OH$** instead, the (TD)DFT calculation results in a mainly localized configuration (Figure S4) that reproduces well the observed spectroscopy (Figure 4).

The TD(DFT) calculated spectroscopy for triplet form for **$Ru^{II}Ru^{IV}O$** redox state reproduces well the observed spectra (Figure 4) and confirms the configuration assigned to this redox state. The two main transitions observed in the visible have a different origin. The more intense band is a result of the superposition of MLCT transitions associated with the {Ru^{II}(tpy)(bpy)}, while the shoulder at lower energies corresponds to at IVCT transition from the Ru(II) to the Ru(IV) (Table 2). The spin density in this redox state is equally distributed among the Ru(IV) and the O atom (Figure S4).

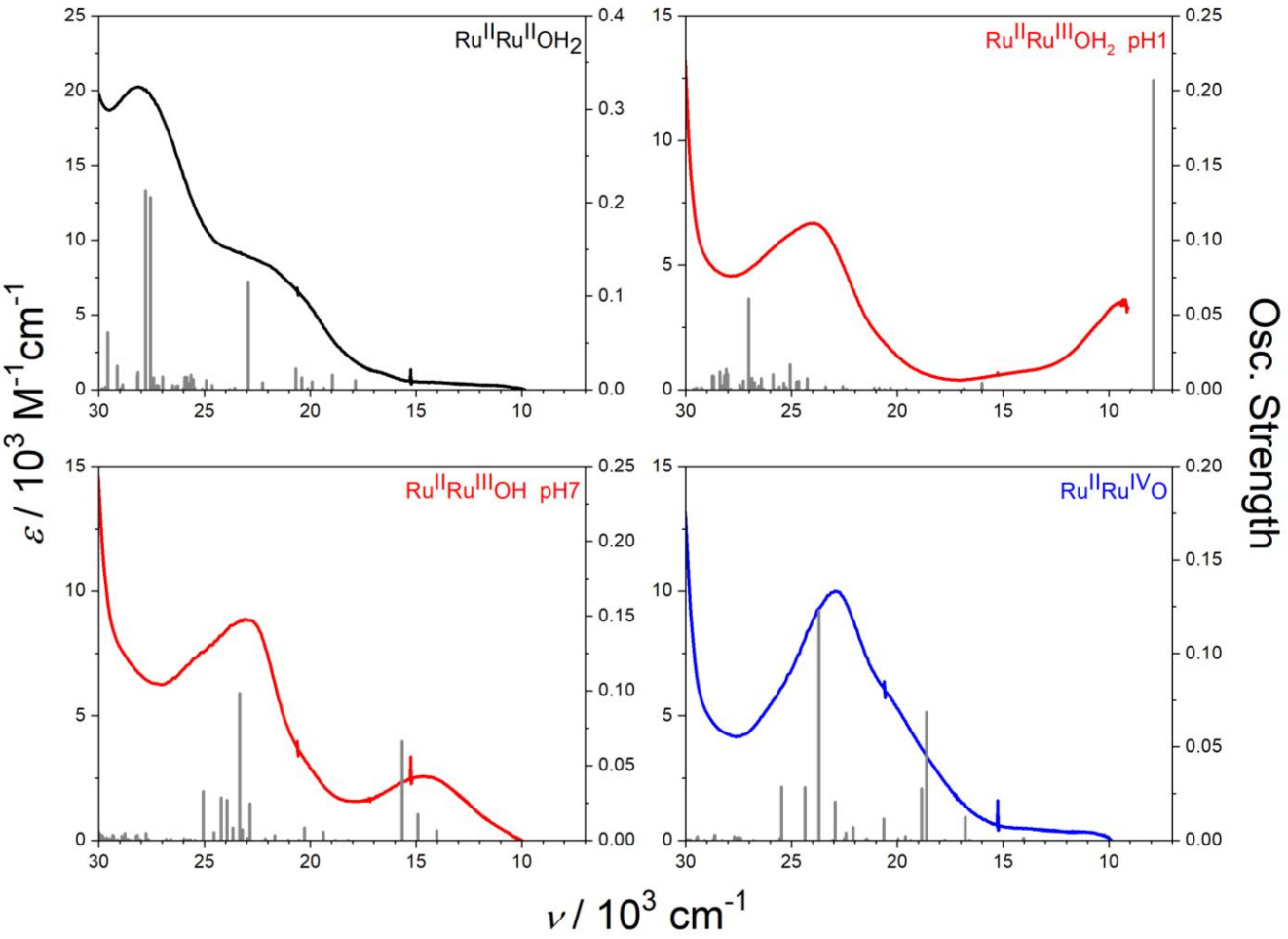

Figure 4. Comparison of the experimental vis-NIR spectra of **$Ru^{II}Ru^{II}OH_2$** (black, pH 1), **$Ru^{II}Ru^{III}OH_2$** (red, pH 1), **$Ru^{II}Ru^{III}OH$** (red, pH 7), **$Ru^{II}Ru^{IV}O$** (blue, pH 1) and the energy of the transitions calculated by (TD)DFT (bars).

Reaction with Ce(IV)

The addition of one to two eq. of Ce(IV) to **$Ru^{II}Ru^{II}OH_2$** at pH 1 results in a very fast reaction and the immediate observation of a spectrum that can interpreted as a mixture of the spectra of **$Ru^{II}Ru^{III}OH_2$** and **$Ru^{II}Ru^{IV}O$** species (Figure S5). Additions of more than two equivalents fail to produce the spectrum of a more oxidized species. Instead, the spectrum is dominated by the bands associated to **$Ru^{II}Ru^{IV}O$** and even after several minutes an absorption begins to grow in the NIR indicating the presence of **$Ru^{II}Ru^{III}OH_2$** in solution. The latter suggests that an oxidized form of the complex is oxidizing the water in a cycle while consuming the oxidation equivalents.

Figure 5 shows the successive spectra for reaction of **$Ru^{II}Ru^{II}OH_2$** with 30 equivalents of Ce(IV) at pH 1. The large excess of the Ce(IV) obscures the bands associated with the complex due the absorbance of the oxidant. This absorbance decreases over time indicating its consumption. This process is accompanied by the appearance of bubbles as expected for the evolution of O_2. After 432 seconds the decay at 370 nm reaches a plateau indicating the end of the consumption of the Ce(IV). Factor analysis of the spectra for this time period indicates that the spectral change is dominated by only one process. Overtime, this band disappears in favour of the spectrum of **$Ru^{II}Ru^{IV}O$** (Figure 5 and S6). At this time, quenching experiments of emission of $[Ru(bpy)_3]^{2+}$ shows the presence of one equivalent of O_2 in the head space of the solution for every four equivalents of Ce(IV) added.

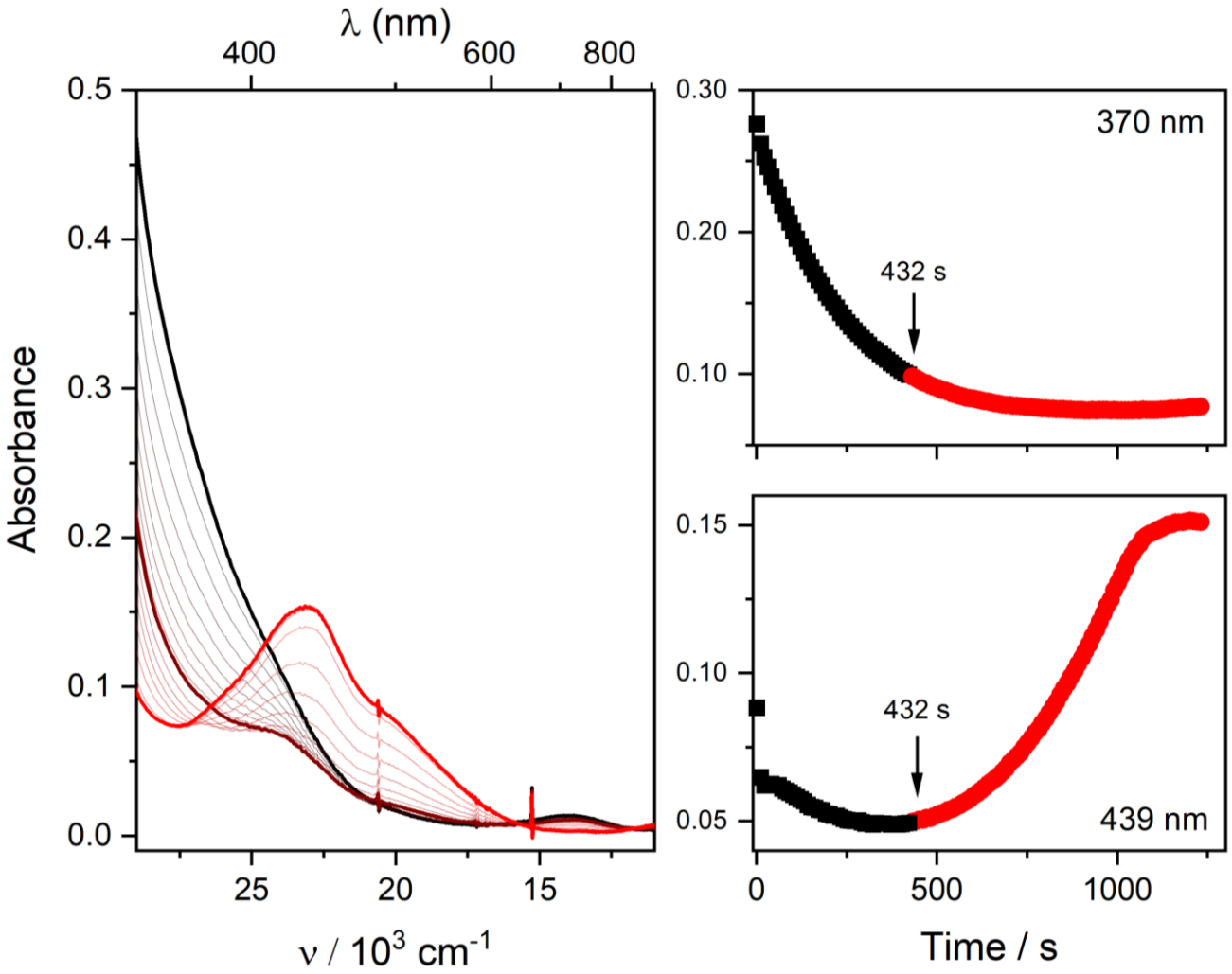

Figure 5. Left: UV-Vis spectral changes upon addition of 30 equivalent of Ce(IV) to a 2×10^{-5} M solution of **$Ru^{II}Ru^{II}OH_2$** in 0.1M $HClO_4$: The initial spectrum (black), the spectrum at 432 seconds and the final spectrum (red) highlighted. Right: Absorbance vs time at 370 nm (top) and 439 nm (bottom).

The observed spectra at the end of initial process (432 seconds, Figure 6), do not present any of the spectroscopic signatures for **$Ru^{II}Ru^{II}OH_2$**, **$Ru^{II}Ru^{III}OH_2$** or **$Ru^{II}Ru^{IV}O$** all of which present distinctive markers in their spectroscopy (Figure 3 and Table 2). Instead, it presents a shoulder at 24700 cm^{-1} and a weak band at 13890 cm^{-1} (720 nm). The lack of an intense MLCT band in the visible suggests that this species has a configuration **$Ru^{III}Ru^{IV}O$**. The weak band at 13890 cm^{-1} is similar to the weak bands observed for the oxidized complexes of the family $[Ru^{III}(tpy)(bpy)(\mu\text{-}CN)Ru^{III}(py)_4L]^{n+}$ (n = 4 or 5 depending on the charge of L).[8] (TD)DFT calculation confirm our assignment and the spectra calculated for this species is very similar to the observed experimentally (Figure 6).

We propose the three-electron oxidized product, **$Ru^{III}Ru^{IV}O$**, as the dominant form of the catalyst involved in the rate determinant step of the the catalytic cycle. Interestingly, a three-electron oxidized product, **$Ru^{V}O$**, has also been proposed as the resting state for the catalytic cycle for $[Ru(tpy)(bpy)OH_2]^{2+}$.[16]

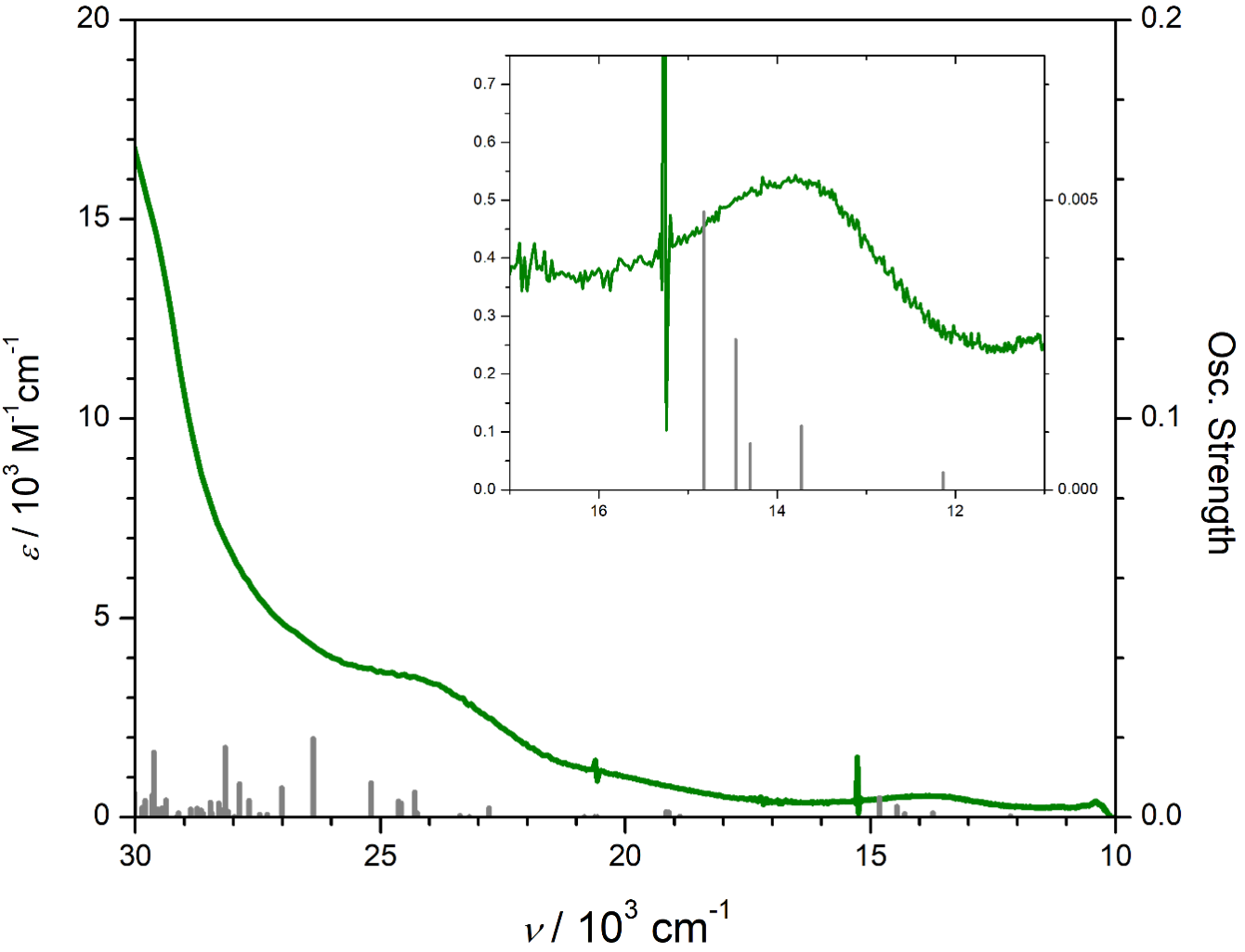

Figure 6. Comparison of the vis-NIR spectrum at 432 seconds for the reaction of 30 equivalent of Ce(IV) and 2×10^{-5} M solution of $Ru^{II}Ru^{II}OH_2$ in 0.1M $HClO_4$ and the energy of the transitions calculated for $Ru^{III}Ru^{IV}O$ by (TD)DFT (bars).

Monitoring the spectral change at 370 nm allowed us to follow the decay of the concentration of Ce(IV) and the kinetics of its consumption. The concentration of **$Ru^{II}Ru^{II}OH_2$** was varied from 5×10^{-6} to 2×10^{-5} M, while Ce(IV) was varied from an excess of 20 to 250 times. The trace at 370 nm follows an exponential decay for several minutes (Figure S7) and the constant for the exponential decay shows a first order in complex (Figure S8). These observations are consistent with the rate law, $-d[Ce^{IV}]/dt = k_{ox}[Ce(IV)][\mathbf{Ru^{II}Ru^{II}OH_2}]$,. From the data in Figure S8, $k_{ox} = 82 \pm 3\ M^{-1}\ s^{-1}$ in 0.1 M $HClO_4$ at 298 K.

Considering all this information, we propose the following mechanism (Scheme 2) for the water oxidation process mediated by **$Ru^{II}Ru^{II}OH_2$**. This mechanism is similar to the proposed for the water oxidation catalysed by other ruthenium polypyridine complexes.[16–18] The key step is the reaction 4 that involves the reaction of **$Ru^{III}Ru^{IV}O$** with Ce(IV). This reaction is also pH sensitive as the cyclic voltammetry experiments show that the irreversible step after the third oxidation is faster at higher pH (Figure 2). This reaction is probably a combination of at least two steps (i) an electron transfer involving the Ce(IV) and (ii) attack of water or OH^- to give a peroxo intermediate. As we do not find evidence for a peroxo intermediate we cannot decide the precise order of these reactions or if it is one concerted step. It has been proposed[16] that the first order in Ce(IV) arises from radical–radical coupling with hydroxocerium(IV) species as the major path leading to the dioxygen formation and the same mechanism could be operative here. It is also interesting to note that another catalyst containing two Ru ions linked presents a rate law for the loss of Ce(IV) that is also first order in both complex and in Ce(IV).[17] Instead, for some cationic complexes, a zero order in Ce(IV) has also been observed.[19,20] In the latter case, the modification of the ligand, that is formation of the O-O, is the slower step.

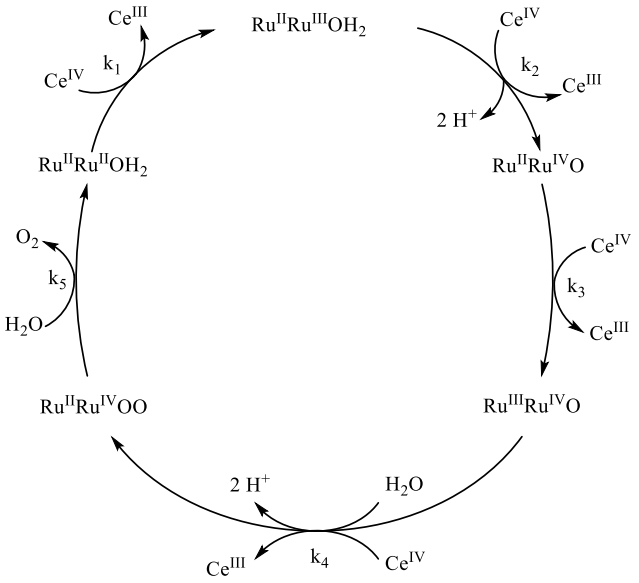

Scheme2. Proposed mechanism for the oxidation of water catalysed by **Ru^{II}Ru^{II}OH$_2$**].

Our results also shows that the **Ru^{III}Ru^{IV}O**$^{3+}$ redox state is not stable. After the consumption of Ce(IV) (Figure 5 and Figure S6b) at 432 seconds, there is a second process that dominates the evolution of the observed spectra. This process involves the growth of the band at 22800 cm^{-1} associated with **Ru^{II}Ru^{IV}O** and the disappearance of the band at 13890 cm^{-1} due to the **Ru^{III}Ru^{IV}O**. Hence, we assign this process to the disproportionation of **Ru^{III}Ru^{IV}O** that results in **Ru^{II}Ru^{IV}O** and the four-electron oxidized product that produces O_2 and **Ru^{II}Ru^{II}OH$_2$**. This assignment is compatible with the observation of a slow chemical step that results in a quasi-reversible behaviour observed for the third oxidation process in the cyclic voltammetry experiments. It is interesting that the three-electron oxidized product can react to give a four-electron product that evolves in the oxidation of water. Given that **Ru^{II}Ru^{IV}O** is a stable product and its oxidation by one electron could result in the accumulation of four equivalents by the disproportionation reaction, it could be an attractive target to carry out the photochemical oxidation of water, as one electron oxidation are a common feature of the reactivity of excited states in general and of Ru polypiridines in particular.

Conclusion

Our results illustrate the effect of adding a strongly coupled redox centre to a catalyst. The second redox centre can store another oxidation equivalent and at the same time activate the catalyst making the **Ru^{IV}O** moiety more reactive. It is also interesting that the **Ru^{III}Ru^{IV}O** oxidation state has a path leading to the four-electron product and the evolution of O_2. As this redox state is available through a one electron oxidation of the stable **Ru^{II}Ru^{IV}O**, it implies that the photooxidation of the latter may be a viable route to the generation of O_2.

Experimental Section

Materials and Synthetic procedures

RuRuOH$_2$(PF$_6$)$_3$ was prepared by a slight modification of the method previously reported[8] (see Supporting Information for details). All other materials were of reagent grade, obtained from commercial sources and used without further purification. All compounds were dried in a vacuum desiccator for at least 12 hours prior to characterization.

Physical measurements. Absorption spectra in the UV-vis/near-IR regions were taken with a Hewlett-Packard 8453 diode array spectrometer (range 190–1100 nm). IR spectra (Figure S2) were recorded with a Nicolet iS10 FT-IR spectrometer (range 4000–400 cm^{-1}). ^{1}H-NMR spectral data (Figure S1) were acquired with a Bruker ARX500 spectrometer, using deuterated solvents from Aldrich. Electrochemical measurements were performed under argon with millimolar solutions of the compounds, using a TEQ V3 potentiostat and a standard three-electrode arrangement consisting of a glassy carbon disc (area = 9.4 mm^2) as the working electrode, a platinum wire as the counter electrode and a commercial Ag/AgCl (3M NaCl) as reference electrode. The supporting electrolyte for pHs above 2 were phosphate buffers with ionic strength 0.1 M, for pH= 1 trifluoroacetic acid 0.1 M with 7 % propylene carbonate

was used, for pH = 2 $HClO_4$ 0.01 M solution with $KClO_4$ added to maintain ionic strength equal to 0.1 M. All the spectroelectrochemical (SEC) experiments were performed using a homemade cell containing a quartz cuvette (1 cm path) where the Ag/AgCl (3M NaCl) electrode was employed as a reference, the working electrode consisted of a Pt mesh and the counter electrode was a Pt wire. The system was entirely purged with Ar. A spectroelectrochemical experiment required the application of an anodic potential for a time that induced charge circulation at the working electrode. Then, the electrolysis was interrupted to allow homogenization of the solution and recording the spectrum. This two-step cycle was repeated several times until advanced reaction progress towards the oxidized species was achieved. The SEC experiment at pH = 1 was done with a $HClO_4$ 0.1 M solution and at pH = 7 a phosphate buffer was used. Ce(IV) solutions were prepared from $(NH_4)_2[Ce(NO_3)_6]$ in $HClO_4$ 0.1. M. Oxygen evolved from the reaction of $\mathbf{Ru^{II}Ru^{II}OH_2}$ with an excess of Ce(IV) was determined measuring the oxygen present in the sample of the headspace of the reaction in a previously purged flask. The sample was collected by gas-tight syringe and injected in a fluorescence cell containing $[Ru(bpy)_3]^{2+}$ in water in absence of oxygen. The concentration of oxygen on the cell was determined measuring the quenching of fluorescence of $[Ru(bpy)_3]^{2+}$. The oxygen evolved in the reaction of $\mathbf{Ru^{II}Ru^{II}OH_2}$ ($1.2 – 3.5 \times 10^{-4}$ M) with an excess of Ce(IV) (150 – 200 equivalents) was at least 80% of the stoichiometric amount considering the added equivalents of Ce(IV).

Computational Methods

Standard Density Functional Theory (DFT) computations were employed to fully optimize the geometries of the complexes in water, without symmetry constraints. The geometry of the Ru(II)-Ru(II) singlet ground state was optimized and served as the starting point for the optimization of the mixed-valence oxidized species. Calculations were done with the *Gaussian09* package,[21] at the B3LYP level of theory using restricted and unrestricted approximations of the Kohn-Sham equations, depending on the total number of electrons.[22] In all cases, we employed the effective core potential basis set LanL2DZ,[23–25] which proved to be suitable for geometry predictions in coordination compounds containing second row transition metals. All the calculations were performed using an UltraFine grid. Solvation effects were accounted for using the most recent implementation of the implicit IEF-PCM solvation model.[26–28] We used tight convergence criteria in the geometry optimizations and default settings for IR calculations. All optimized structures were confirmed as minima by analysing the harmonic vibrational frequencies.[29] Vertical electronic excitation energies and intensities were evaluated using time-dependent DFT ((TD)DFT)[30,31] approach with the *Gaussian09* package,[21] without symmetry constraints. GaussSum 2.2.6[32] software was used to perform spectral simulations, to extract spectral data and molecular orbital information and to obtain the electron density difference maps (EDDM). Graphical visualizations were generated by GaussView5.0.8,[33] i.e., the isovalues were drawn at 0.004 (EDDM), 0.04 (Kohn−Sham MOs), or 0.004 (spin-density calculations). The EDDM, the composition of electronic transitions, and the associated molecular orbitals for all the calculated complexes are shown in the Supporting Information. An asset of our methodology is the excellent balance between adequate descriptions of the electronic structures and low associated computational costs. In our experience, the use of larger basis sets, does not lead to improved results for cyanide-bridge ruthenium polypyridine systems.[15]

Acknowledgements

This work was partially supported by the University of Buenos Aires, CONICET (PIP 0659) and ANPCyT (PICT-2017-1018). The authors gratefully thank Dra. Paola Oviedo for providing the initial samples of the complex studied here and Dr. Leonardo Slep and Lic. Julián Perdoménico for their help with SEC experiments. LBV and GEP are members of the scientific staff of CONICET and SED and MVJ acknowledges fellowship support from the same institution. GEP thanks Prof. Dr Adrián Roitberg for selflessly sharing his knowledge.

Keywords: Cyanide Bridge • Homogeneous Catalysis • Metal Metal Interaction • Ruthenium • Water Oxidation

[1] N. S. Lewis, *Nat. Nanotechnol.* **2016**, *11*, 1010–1019.

[2] X. Sala, S. Maji, R. Bofill, J. García-Antón, L. Escriche, A. Llobet, *Acc. Chem. Res.* **2014**, *47*, 504–516.

[3] P. Garrido-Barros, D. Moonshiram, M. Gil-Sepulcre, P. Pelosin, C. Gimbert-Suriñach, J. Benet-Buchholz, A. Llobet, *J. Am. Chem. Soc.* **2020**, *142*, 17434–17446.

[4] B. Zhang, L. Sun, *J. Am. Chem. Soc.* **2019**, *141*, 5565–5580.

[5] R. Matheu, M. Z. Ertem, C. Gimbert-Suriñach, X. Sala, A. Llobet, *Chem. Rev.* **2019**, *119*, 3453–3471.

[6] J. J. Concepcion, M. K. Tsai, J. T. Muckerman, T. J. Meyer, *J. Am. Chem. Soc.* **2010**, *132*, 1545–1557.

[7] J. Yang, L. Wang, S. Zhan, H. Zou, H. Chen, M. S. G. M. S. G. Ahlquist, L. Duan, L. Sun, *Nat. Commun.* **2021**, *12*, 373.

[8] S. E. Domínguez, G. E. Pieslinger, L. Sanchez-Merlinsky, L. M. Baraldo, *Dalt. Trans.* **2020**, *49*, 4125–4135.

[9] P. S. Oviedo, G. E. Pieslinger, A. Cadranel, L. M. Baraldo, *Dalt. Trans.* **2017**, *46*, 15757–15768.

[10] G. E. Pieslinger, P. Alborés, L. D. Slep, L. M. Baraldo, *Angew. Chemie Int. Ed.* **2014**, *53*, 1293–1296.

[11] M. B. Rossi, K. A. Abboud, P. Alborés, L. M. Baraldo, *Eur. J. Inorg. Chem.* **2010**, *2010*, 5613–5616.

[12] E. L. Lebeau, R. A. Binstead, T. J. Meyer, *J. Am. Chem. Soc.* **2001**, *123*, 10535–10544.

[13] M. B. Rossi, O. E. Piro, E. E. Castellano, P. Alborés, L. M. Baraldo, *Inorg. Chem.* **2008**, *47*, 2416–27.

[14] G. E. Pieslinger, B. M. Aramburu-Trošelj, A. Cadranel, L. M. Baraldo, *Inorg. Chem.* **2014**, *53*, 8221–8229.

[15] G. E. Pieslinger, A. Cadranel, L. M. Baraldo, *J. Braz. Chem. Soc.* **2020**, *31*, 2360–2370.

[16] A. Kimoto, K. Yamauchi, M. Yoshida, S. Masaoka, K. Sakai, *Chem. Commun.* **2012**, *48*, 239–241.

[17] M. R. Norris, J. J. Concepcion, D. P. Harrison, R. A. Binstead, D. L. Ashford, Z. Fang, J. L. Templeton, T. J. Meyer, *J. Am. Chem. Soc.* **2013**, *135*, 2080–2083.

[18] M. Yoshida, S. Masaoka, J. Abe, K. Sakai, *Chem. - An Asian J.* **2010**, *5*, 2369–2378.

[19] J. J. Concepcion, J. W. Jurss, J. L. Templeton, T. J. Meyer, *J. Am. Chem. Soc.* **2008**, *130*, 16462–16463.

[20] J. J. Concepcion, J. W. Jurss, M. R. Norris, Z. Chen, J. L. Templeton, T. J. Meyer, *Inorg. Chem.* **2010**, *49*, 1277–1279.

[21] *Gaussian 09, Revision D.01*, M. J. Frisch, G. W. Trucks, H. B. Schlegel, G. E. Scuseria, M. A. Robb, J. R. Cheeseman, G. Scalmani, V. Barone, B. Mennucci, G. A. Petersson, H. Nakatsuji, M. Caricato, X. Li, H. P. Hratchian, A. F. Izmaylov, J. Bloino, G. Zheng, J. L. Sonnenberg, M. Hada, M. Ehara, K. Toyota, R. Fukuda, J. Hasegawa, M. Ishida, T. Nakajima, Y. Honda, O. Kitao, H. Nakai, T. Vreven, J. A. Montgomery, Jr., J. E. Peralta, F. Ogliaro, M. Bearpark, J. J. Heyd, E. Brothers, K. N. Kudin, V. N. Staroverov, T. Keith, R. Kobayashi, J. Normand, K. Raghavachari, A. Rendell, J. C. Burant, S. S. Iyengar, J. Tomasi, M. Cossi, N. Rega, J. M. Millam, M. Klene, J. E. Knox, J. B. Cross, V. Bakken, C. Adamo, J. Jaramillo, R. Gomperts, R. E. Stratmann, O. Yazyev, A. J. Austin, R. Cammi, C. Pomelli, J. W. Ochterski, R. L. Martin, K. Morokuma, V. G. Zakrzewski, G. A. Voth, P. Salvador, J. J. Dannenberg, S. Dapprich, A. D. Daniels, O. Farkas, J. B. Foresman, J. V. Ortiz, J. Cioslowski, and D. J. Fox, Gaussian, Inc., Wallingford CT, **2013**.

[22] A. Szabo, N. S. Ostlund, *Modern Quantum Chemistry: Introduction to Advanced Electronic Structure Theory*, New York, **1996**.

[23] W. R. Wadt, P. J. Hay, *J. Chem. Phys.* **1985**, *82*, 284–298.

[24] T. H. Dunning, P. J. Hay, in *Methods Electron. Struct. Theory* (Ed.: H.F. Schaefer), Springer US, Boston, MA, **1977**, pp. 1–27.

[25] P. J. Hay, W. R. Wadt, *J. Chem. Phys.* **1985**, *82*, 299–310.

[26] G. Scalmani, M. J. Frisch, *J. Chem. Phys.* **2010**, *132*, 114110.

[27] J. Tomasi, B. Mennucci, R. Cammi, *Chem. Rev.* **2005**, *105*, 2999–3094.

[28] S. Miertuš, E. Scrocco, J. Tomasi, *Chem. Phys.* **1981**, *55*, 117–129.

[29] H. B. Schlegel, *J. Comput. Chem.* **1982**, *3*, 214–218.

[30] L. Petit, P. Maldivi, C. Adamo, *J. Chem. Theory Comput.* **2005**, *1*, 953–962.

[31] R. E. Stratmann, G. E. Scuseria, M. J. Frisch, *J. Chem. Phys.* **1998**, *109*, 8218–8224.

[32] N. M. O'Boyle, A. L. Tenderholt, K. M. Langner, *J. Comput. Chem.* **2008**, *29*, 839–845.

[33] GaussView, Version 5.0.8, R. Dennington, T. Keith, J. Millam, Semichem Inc., Shawnee Mission, KS, **2009**.

10.1002/ejic.202100843

Entry for the Table of Contents

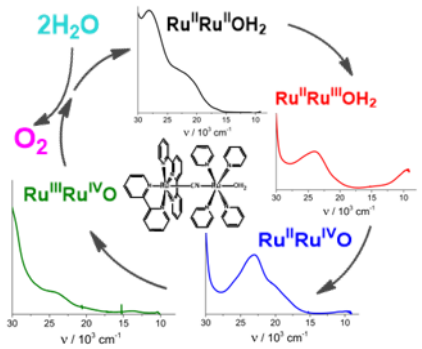

A strongly coupled biruthenium complex is shown to be an active catalyst for water oxidation. The rich spectroscopy of these complexes allowed us to characterize the redox states involved in this reaction. The rate-determining step is the oxidation of the three-electron oxidized product that has a configuration $Ru^{III}Ru^{IV}O$.

Institute and/or researcher Twitter usernames: @luisbaraldo